

P. Ikonen, P. Belov, C. Simovski, and S. Maslovski, Experimental demonstration of subwavelength field channeling at microwave frequencies using a capacitively loaded wire medium, *Physical Review B*, vol. 73, 073102, 2006.

© 2006 American Physical Society

Reprinted with permission.

Readers may view, browse, and/or download material for temporary copying purposes only, provided these uses are for noncommercial personal purposes. Except as provided by law, this material may not be further reproduced, distributed, transmitted, modified, adapted, performed, displayed, published, or sold in whole or part, without prior written permission from the American Physical Society.

<http://link.aps.org/abstract/prb/v73/p073102>

Experimental demonstration of subwavelength field channeling at microwave frequencies using a capacitively loaded wire medium

Pekka Ikonen,¹ Pavel Belov,^{2,3} Constantin Simovski,^{1,3} and Stanislav Maslovski¹

¹Radio Laboratory/SMARAD, Helsinki University of Technology, P.O. Box 3000, FI-02015 TKK, Finland

²Queen Mary College, University of London, Mile End Road, London E1 4NS, United Kingdom

³Photonics and Optoinformatics Department, St. Petersburg State University of Information Technologies, Mechanics and Optics, Sablinskaya 14, 197101, St. Petersburg, Russia

(Received 5 December 2005; published 1 February 2006)

In this Brief Report we experimentally demonstrate a possibility to channel the near field distribution of a line source with sub-wavelength details through a layer of an electromagnetic crystal. Channeled intensity maximum having radius of $\lambda/10$ has been obtained using an electrically dense lattice of capacitively loaded wires. The loading allows us to reduce the lattice period dramatically so that it is only a small fraction of the free-space wavelength. It is shown that losses in the structure only decrease the total amplitude of the channeled intensity distribution, but do not influence the details.

DOI: [10.1103/PhysRevB.73.073102](https://doi.org/10.1103/PhysRevB.73.073102)

PACS number(s): 78.20.Ci, 41.20.Jb, 42.70.Qs

It was theoretically shown by Notomi¹ and experimentally proven by Parimi *et al.*² that in photonic crystals (PC) or electromagnetic crystals (EC) negative refraction can be achieved at frequencies close to the electromagnetic band-gap edges. Developing this direction of studies, Luo *et al.* introduced a flat *superlens* formed by a slab of PC in Ref. 3, and studied theoretically the possibility for sub-wavelength imaging in a layer of EC Ref. 4. Recently, it has been shown that with PC/EC based structures neither negative refraction or surface plasmon excitation is required to obtain a point source image whose size is smaller than $\lambda/2$. In this case the subwavelength image size has theoretically been achieved when the crystal iso-frequency contour has a special (flat) shape.⁵⁻⁹ In this letter we experimentally validate the recently proposed concept of *sub-wavelength field channeling*⁹ that explains the aforementioned effect by a transformation of evanescent modes into propagating crystal eigenmodes, and describes a special regime for the wave propagation. This regime has been called in the literature as *self collimation*,⁵ *directed diffraction*,⁶ *tunneling*,⁷ *absolute negative refraction*,⁸ and *self-guiding*.¹⁰ In subwavelength field channeling the crystal slab effectively operates as a transmission device transferring the near field distribution of a source from the front interface to the back interface. It is conceptually important to note that the slab is not a lens in the optical point of view, and that no focusing is incorporated to the phenomenon. When the slab operates within the channeling regime and the source is located close to the front interface, the evanescent free-space harmonics transform into propagating crystal eigenmodes at the first crystal interface.⁹ The near field distribution of the source is carried by these eigenmodes to the back interface where it diffracts into the free space (the second crystal interface can be thought as an aperture radiator with the channeled near field distribution corresponding to the aperture distribution). Very close to the back interface the channeled distribution can be detected.

The crystal structures used to theoretically demonstrate the sub-wavelength field channeling include lattices of dielectric rods^{5,7} and lattices of metal rods coated with high-

permittivity dielectrics.⁸ We propose to utilize *capacitively loaded wire medium* (CLWM)¹¹ for implementing the operational regime, see Fig. 1(a). Compared to conventional wire medium¹² or lattices of dielectric rods, CLWM offers additional features which make it superior in design. Authors of Ref. 11 have shown that CLWM has a band-gap near the resonant frequency of a single capacitively loaded wire (the so called *resonant band-gap*). By changing the value of the load capacitance, the location of this band-gap can be conveniently tuned. Moreover, a high value of capacitance allows us to locate the resonant band-gap significantly below the first lattice resonance, thus the needed regime can be achieved with an electrically dense lattice. Obviously, the details of the channeled distribution are restricted by the lattice period. Thus, the more (electrically) dense is the lattice, the finer can be the details of the channeled distribution.

For implementing the proposed regime we use the following geometry and structural dimensions (see Fig. 1): The lattice period $a=10$ mm, the radius of wires $r_0=0.058a$, the insertion period for the loads $c=2.2a$, and loading capacitance $C_0=0.5$ pF. The crystal sample has dimensions $N_l=14$ and $N_t=21$, where N_l is the number of rows of wires, and N_t is the number of columns of wires. $N_l=14$ is chosen to meet the Fabry-Pérot resonance (FPR) condition at the

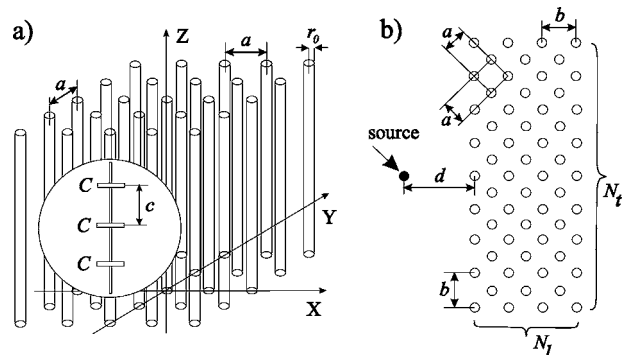


FIG. 1. (a) Geometry of capacitively loaded wire medium (CLWM). (b) Geometry of the crystal sample.

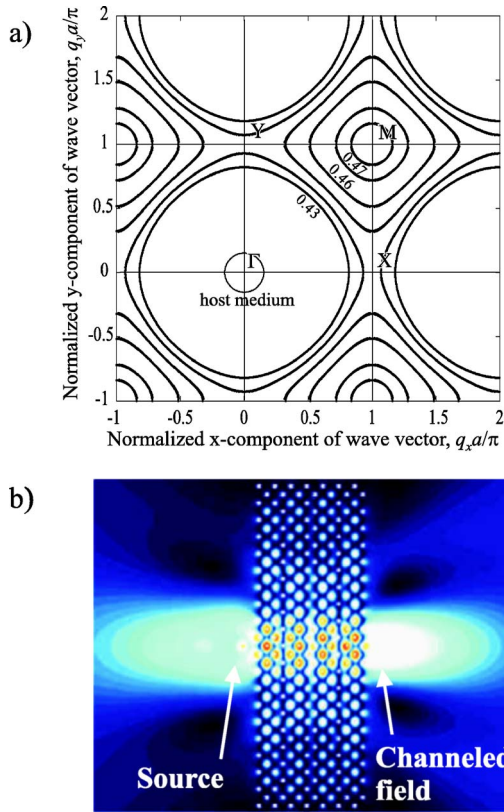


FIG. 2. (Color online) (a) Isofrequency contours for CLWM. The numbers correspond to values of normalized frequency ka . (b) Simulated intensity distribution.

normalized frequency $ka=0.46$,⁹ where k is the wave number in free space ($a/\lambda=0.073$). Figure 2(a) shows isofrequency contours for the frequency region near the lower edge of the resonant band-gap. The isofrequency contour of the host matrix for $ka=0.46$ is shown as the small circle around Γ point. The part of the isofrequency contour of the crystal corresponding to $ka=0.46$, and located within the first Brillouin zone, is practically flat. This part is perpendicular to the diagonal of the first Brillouin zone. Thus, in order to achieve channeling regime we orient interfaces of the slab orthogonally to (11)-direction of the crystal as shown in Fig. 1(b). Figure 2(b) depicts the simulated intensity distribution when using a line source as excitation.⁹ There is a clear channel through the slab indicating the propagation of the excited crystal eigenmodes. A bright spot having a radius of $\lambda/6$ [determined from the intensity distribution at level $\max(\text{intensity})/2$] is seen behind the slab.

Figure 3(a) shows a photograph of the implemented CLWM sample. To ease the fabrication, the capacitively loaded wires are implemented as printed strips on top of FR4-substrate [relative permittivity $\epsilon_r \sim 4.5(1-j0.01)$, thickness of the plates is 1.0 mm]. According to numerical simulations, losses introduced by the rather low quality substrate are within an acceptable range. Thus, despite the lowered transmission level at the desired FPR, the achieved intensity distribution should be only moderately disturbed. To implement the desired distributed capacitance level we utilize the structure shown in Fig. 3(b). Since the transverse thickness

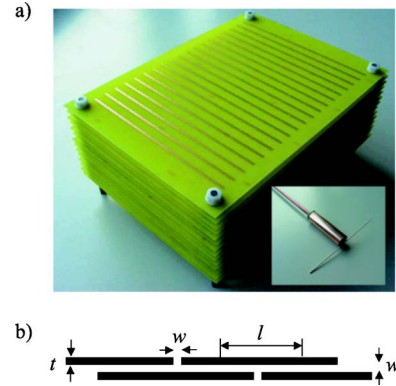


FIG. 3. (Color online) (a) The implemented CLWM crystal sample and the probe used in the measurements. (b) A schematic illustration of the loaded wire (a piece of it).

of the structure (strip) is very small, the incoming wave sees the structure as a continuous C -loaded strip. Also, in this structure the capacitance is well distributed along the strip leading to highly uniform current distribution. Estimated dimensions for the structure to produce the desired distributed capacitance level of $11 \text{ fF}\cdot\text{m}$ are $l=22.0 \text{ mm}$, $t=0.575 \text{ mm}$, and $w=1.1 \text{ mm}$ [see Fig. 3(b)].

The measurement setup is schematically depicted in Fig. 4(a). The source and the probe used to scan the field distribution are connected to a vector network analyzer (VNA). The probe holder is connected to a control box responsible for the movement of the probe. VNA contains an in-house

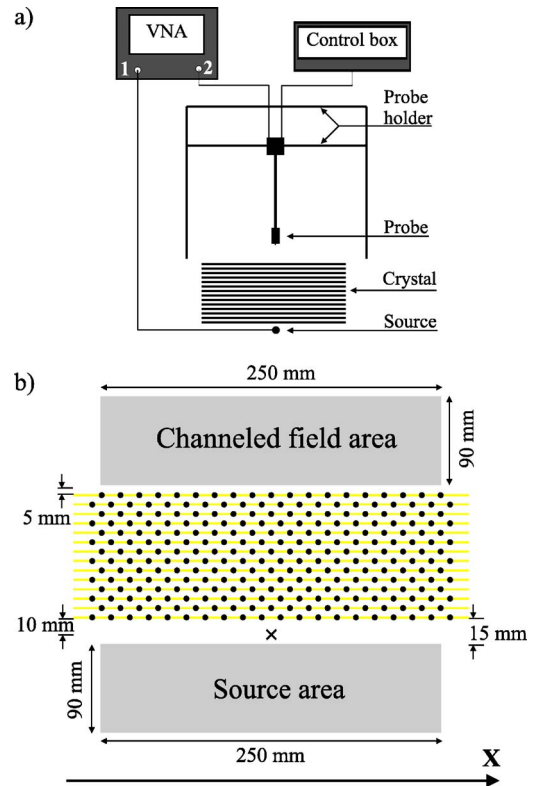


FIG. 4. (Color online) (a) A schematic illustration of the measurement setup. (b) The measurement area. The black dots denote the loaded strips, the cross denotes the source.

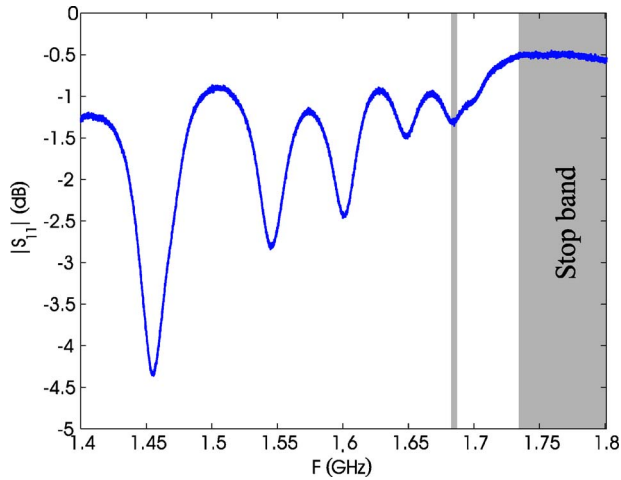


FIG. 5. (Color online) Measured S_{11} -level of the slab. The desired Fabry-Pérot resonance is shown with a vertical line.

program for recording electric field values. To maximize the sensitivity of the measurement setup, the source and the probe are both based on resonant dipoles operating at the measured FPR [see Fig. 3(a) for a photograph of the probe]. Figure 4(b) shows the measurement areas and the orientation of the CLWM crystal during the measurements. The spatial step of the probe is 5 mm.

First, we need to locate the desired FPR for which the slab has been tuned. This frequency lies approximately at the lower edge of the first crystal stop band. To locate the FPR we measure the reflection level from the slab using a wide-band horn. The result is presented in Fig. 5. Undoubtedly, there are strong near field interactions between the slab and the horn, therefore, Fig. 5 does not properly show the true reflection properties of the slab. Nevertheless, the stop band edge at 1.73 GHz, and the FPR at 1.684 GHz are seen in Fig. 5: Only a traveling wave is capable of producing the resonant peaks shown in Fig. 5. Inside the stop-band of the structure a wave decays exponentially and the amplitude of the reflection coefficient approaches unity. Thus, when the resonant peaks are not seen and the reflection coefficient amplitude is close to unity we have found the stop-band edge.

The dielectric plates have a visible influence on the transmission characteristics: The lower edge of the resonant stop band has shifted from the predicted (for wires in free space) 2.20⁹ to 1.73 GHz. Consequently, there is most likely some discrepancy in the estimated parameters used to predict the capacitance level. From the measured location of the lower stop band edge we estimate that effectively the distributed capacitance level at the FPR is 17.6 fF·m. According to the numerical simulations, higher capacitance level makes the details of the channeled distribution finer.

The following measurements have been performed at frequency 1.684 GHz which corresponds to the FPR identified from the reflection measurement. Figure 6(a) shows the measured intensity distribution in the source and the channeled field area. We can observe that there is a clear and symmetrical spot behind the slab. The radius of the intensity spot (determined at level $\max(\text{intensity})/2$) is approximately 0.10λ , thus we are dealing with a significant sub-wavelength

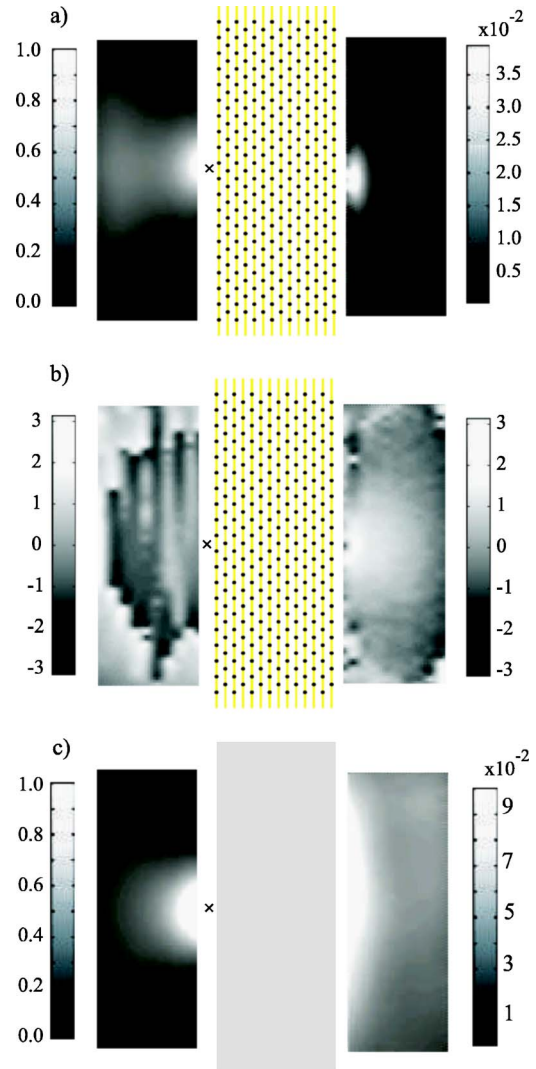


FIG. 6. (Color online) (a) The measured intensity distribution (in arb. units). (b) The measured phase distribution of electric field (in radians). (c) The measured intensity distribution without the CLWM crystal (in arb. units). In (a) and (c) the intensity values in the channeled field area have not been normalized to better see the details of the intensity distribution.

resolution. It is worth noticing that due to the nature of the measurement probe, the probe is inherently incapable of averaging the detected transmitted field (as is the case, e.g., with loop detectors¹³). Since the dipole arm is very thin, the exact distribution of the transmitted field can be very accurately measured, and the details of the distribution hardly depend on the electrical size of the probe. Contrary to the simulations, we can observe from Fig. 6(a) that as the probe moves closer to the slab interface, the field strength slightly decreases. This is most likely caused by destructive interaction between the metal parts of the probe and the metal strips leading to the loss of the resonant condition in the vicinity of the wire surface (similar effect has been observed with loop shaped metal particles and loop shaped metal detector¹³).

The measured phase distribution of the electric field is presented in Fig. 6(b). In the channeled field area we can identify the phase front of a wave diverging from output

interface of the crystal. In the source area the phase distribution is disturbed by reflections from the slab. Figure 6(c) shows the measured intensity distribution without the crystal (the shadowed region shows the space previously occupied by the slab). Slight asymmetry is seen in the cylindrical intensity profile. This weak asymmetry is expected to be caused by parasitic currents induced to the balun of the source probe (the transversal thickness of the balun is not negligible). The effect of parasitic radiation is not seen in the source area when the field level produced by the dipole radiation is strong. Moreover, the parasitic radiation does not destroy the symmetry of the intensity profile when the slab is present. This is due to the fact that outside the channel the field level is very low (most of the energy flows inside the channel). Thus, the parasitic radiation directed away from the symmetry axis of the slab attenuates rapidly before approaching the channeled field area.

The measured transversal intensity distributions are shown in Fig. 7 [see Fig. 4(b) for definition of the coordinate system]. The measured maximum field value is approximately 35% lower when using the crystal slab than in the free space measurement. The biggest reason for this degradation is the strong reflection occurring at the first crystal interface. The lossy dielectric plates also degrade the amplitude level of the channeled field. It is important to note, however, that the details of the distribution are not affected by the losses. This important practical property is inherent to the subwavelength field channeling: The propagating waves in a lossy material experience the same decay irrespective of their transversal wave vector components which are responsible for the shape of the channeled field distribution.

In the present letter we have experimentally validated the concept of sub-wavelength field channeling using a slab of an electromagnetic crystal. It has been shown that losses influence only to the total amplitude of the channeled field distribution, but do not disturb its shape. We have shown that an intensity spot with radius of $\lambda/10$ can be achieved using an electrically dense lattice of capacitively loaded wires. The

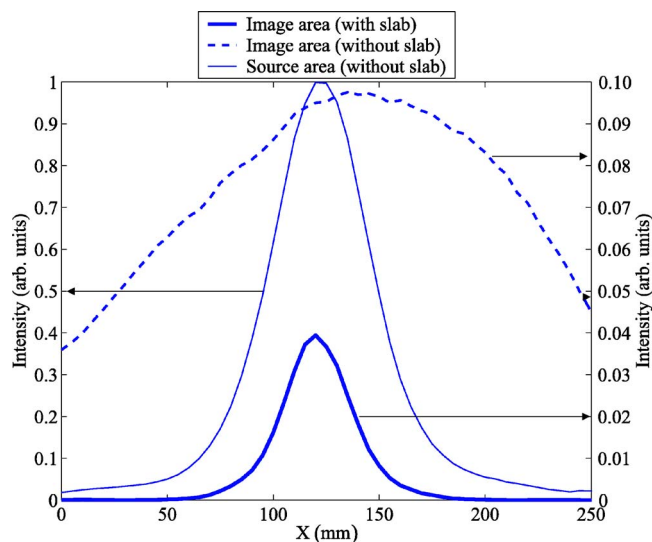


FIG. 7. (Color online) Measured intensity distribution along the axis x (parallel to the slab interface). The arrow indicates the scale which is used to read the intensity values. Intensity in the channeled field area has been measured at 10 mm distance from the slab interface. Intensity in the source area has been measured at 10 mm distance from the source.

spot size is noticeably below the theoretical diffraction limit, and it is twice smaller than the minimum image size practically obtained in the modern high-precision microscopy. Compared to the results obtained in the optical regime,¹⁴ the radius of the channeled intensity spot is two times smaller than the reported image size in Ref. 14. In the microwave regime the proposed structure could be used as a wave channel multiplexer or a decoupler for antenna systems.

Useful discussions with Sergei Tretyakov are acknowledged. One of the authors (P.I.) wishes to thank Eino Kahra from the Radio Laboratory TKK for assistance in manufacturing the prototype.

¹M. Notomi, Phys. Rev. B **62**, 10696 (2000).

²P. V. Parimi, W. T. Lu, P. Vodo, and S. Sridhar, Nature (London) **426**, 404 (2003).

³C. Luo, S. G. Johnson, J. D. Joannopoulos, and J. Pendry, Phys. Rev. B **65**, 201104(R) (2002).

⁴C. Luo, S. G. Johnson, J. D. Joannopoulos, and J. Pendry, Phys. Rev. B **68**, 045115 (2003).

⁵Z.-Y. Li and L.-L. Lin, Phys. Rev. B **68**, 245110 (2003).

⁶H.-T. Chien, H.-T. Tang, C.-H. Kuo, C.-C. Chen, and Z. Ye, Phys. Rev. B **70**, 113101 (2004).

⁷C.-H. Kuo and Z. Ye, Phys. Rev. E **70**, 056608 (2004).

⁸X. Zhang, Phys. Rev. B **70**, 205102 (2004).

⁹P. A. Belov, C. R. Simovski, and P. Ikonen, Phys. Rev. B **71**, 193105 (2005).

¹⁰D. N. Chigrin, S. Enoch, C. M. S. Torres, and G. Tayeb, Opt. Express **11**, 1203 (2003).

¹¹P. A. Belov, C. R. Simovski, and S. A. Tretyakov, Phys. Rev. E **66**, 036610 (2002).

¹²N. A. Nicorovici, R. C. McPhedran, and L. C. Botten, Phys. Rev. E **52**, 1135 (1995).

¹³R. Marqués, F. Martín, and M. Sorolla, Proc. Latsis Symposium pp. 50–53 (2005).

¹⁴N. Fang, H. Lee, C. Sun, and X. Zhang, Science **308**, 534 (2005).